iScience

CellPress
OPEN ACCESS

Article

Cancer cell immune mimicry delineates onco-immunologic modulation

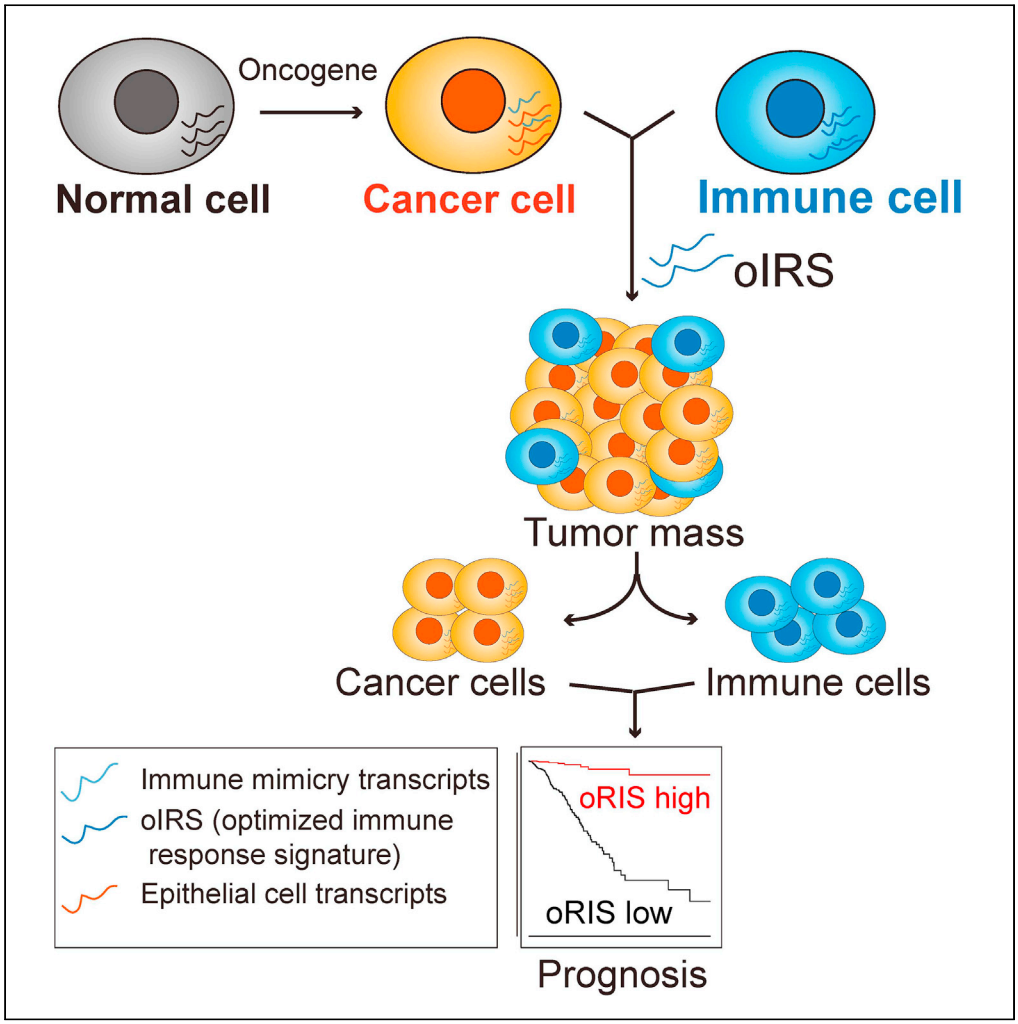

Rui Gao, Bin He, Qitao Huang, ..., Suxia Lin, Bo Wang, Quentin Liu

linsx@sysucc.org.cn (S.L.)
wangb76@mail.sysu.edu.cn (B.W.)
liuq9@mail.sysu.edu.cn (Q.L.)

Highlights

Single-cell transcriptome reveals immune mimicry as a distinct cancer hallmark

Mimicry transcripts contribute to distinct prognoses of immune gene signatures

oIRS refines prognostic evaluation and points to core favorable immune processes

oIRS signifies the role of antigen presentation and indicates immunotherapy response

Gao et al., iScience *24*, 103133
October 22, 2021
https://doi.org/10.1016/j.isci.2021.103133

iScience

CellPress
OPEN ACCESS

Article

Cancer cell immune mimicry delineates onco-immunologic modulation

Rui Gao,[1,2] Bin He,[2] Qitao Huang,[2] Zifeng Wang,[2] Min Yan,[2] Eric Wing-Fai Lam,[4] Suxia Lin,[2,*] Bo Wang,[1,*] and Quentin Liu[1,2,3,5,*]

SUMMARY

Immune transcripts are essential for depicting onco-immunologic interactions. However, whether cancer cells mimic immune transcripts to reprogram onco-immunologic interaction remains unclear. Here, single-cell transcriptomic analyses of 7,737 normal and 37,476 cancer cells reveal increased immune transcripts in cancer cells. Cells gradually acquire immune transcripts in malignant transformation. Notably, cancer cell-derived immune transcripts contribute to distinct prognoses of immune gene signatures. Optimized immune response signature (oIRS), obtained by excluding cancer-related immune genes from immune gene signatures, and offers a more reliable prognostic value. oIRS reveals that antigen presentation, NK cell killing and T cell signaling are associated with favorable prognosis. Patients with higher oIRS expression are associated with favorable responses to immunotherapy. Indeed, CD83^{+} cell infiltration, which indicates antigen presentation activity, predicts favorable prognosis in breast cancer. These findings unveil that immune mimicry is a distinct cancer hallmark, providing an example of cancer cell plasticity and a refined view of tumor microenvironment.

INTRODUCTION

Emerging evidence suggests that cancer cells acquire differentiation programs of distinct cell types, including vascular (Maniotis et al., 1999), neuron (Zeng et al., 2019) and immune (Gangoso et al., 2021) cell programs to facilitate tumor progression. However, this cancer cell-intrinsic differentiation plasticity is indistinguishable from tumor-infiltrated microenvironmental cells by conventional transcriptomic profiling of bulk tumors. The differentiation plasticity thus poses challenges to characterizing tumor immune microenvironment, which is critical for the development of effective therapeutic approaches, especially immunotherapy (Salmon et al., 2019). Recently, expansion in single cell RNA sequencing (scRNA-seq) datasets of both cancer and immune compartments provides a unique opportunity to define single cell differentiation status and refine the tumor immune landscape (Chung et al., 2017; Filbin et al., 2018; Francesconi et al., 2019; Gangoso et al., 2021; Kim et al., 2015; Muraro et al., 2016; Ouadah et al., 2019; Vuong et al., 2018). However, the presence of immune-like programs in cancer cells, which might rewire the immune microenvironment, remains poorly defined.

The immune cell activity in the tumor microenvironment is currently inferred from the transcriptomic profiles of the bulk tumor tissues (Gentles et al., 2015; Gorenshteyn et al., 2015; He et al., 2019; Newman et al., 2015). For instance, the tumor transcriptomic profiles are used to determine the clinical significance of tumor infiltrated immune cells in patients (Gentles et al., 2015). Recently, a growing number of tumor-profiling resources such as the Cancer Genome Atlas (TCGA) project (Weinstein et al., 2013) has characterized the genomic, transcriptomic, and epigenomic profiles in thousands of human tumors. However, immune activities, indicated by individual markers or gene signatures, are often associated with distinct clinical outcomes in different cancer types (Bruni et al., 2020). The mechanism underlying these inconsistencies is poorly understood, and the involvement of cancer cell plasticity in the immune microenvironment remains to be determined.

Immune processes play distinct roles in cancer. For instance, processes that direct tumor cells killing by natural killer (NK) cells and CD8 T cells are generally tumor-suppressing (Havel et al., 2019; Salmon et al., 2019; Shimasaki et al., 2020), whereas those suppressing antitumor NK cells and T cells by regulatory T cells or

[1]Department of Medical Oncology, The Seventh Affiliated Hospital, Sun Yat-sen University, Shenzhen 510275, P.R. China

[2]State Key Laboratory of Oncology in South China, Collaborative Innovation Center of Cancer Medicine, Sun Yat-sen University Cancer Center, Guangzhou 510060, P.R. China

[3]Institute of Cancer Stem Cell, Dalian Medical University, Dalian 116044, P.R. China

[4]Department of Surgery and Cancer, Imperial College London, Hammersmith Hospital Campus, London, W12 ONN, UK

[5]Lead contact

*Correspondence: linsx@sysucc.org.cn (S.L.), wangb76@mail.sysu.edu.cn (B.W.), liuq9@mail.sysu.edu.cn (Q.L.)

https://doi.org/10.1016/j.isci.2021.103133

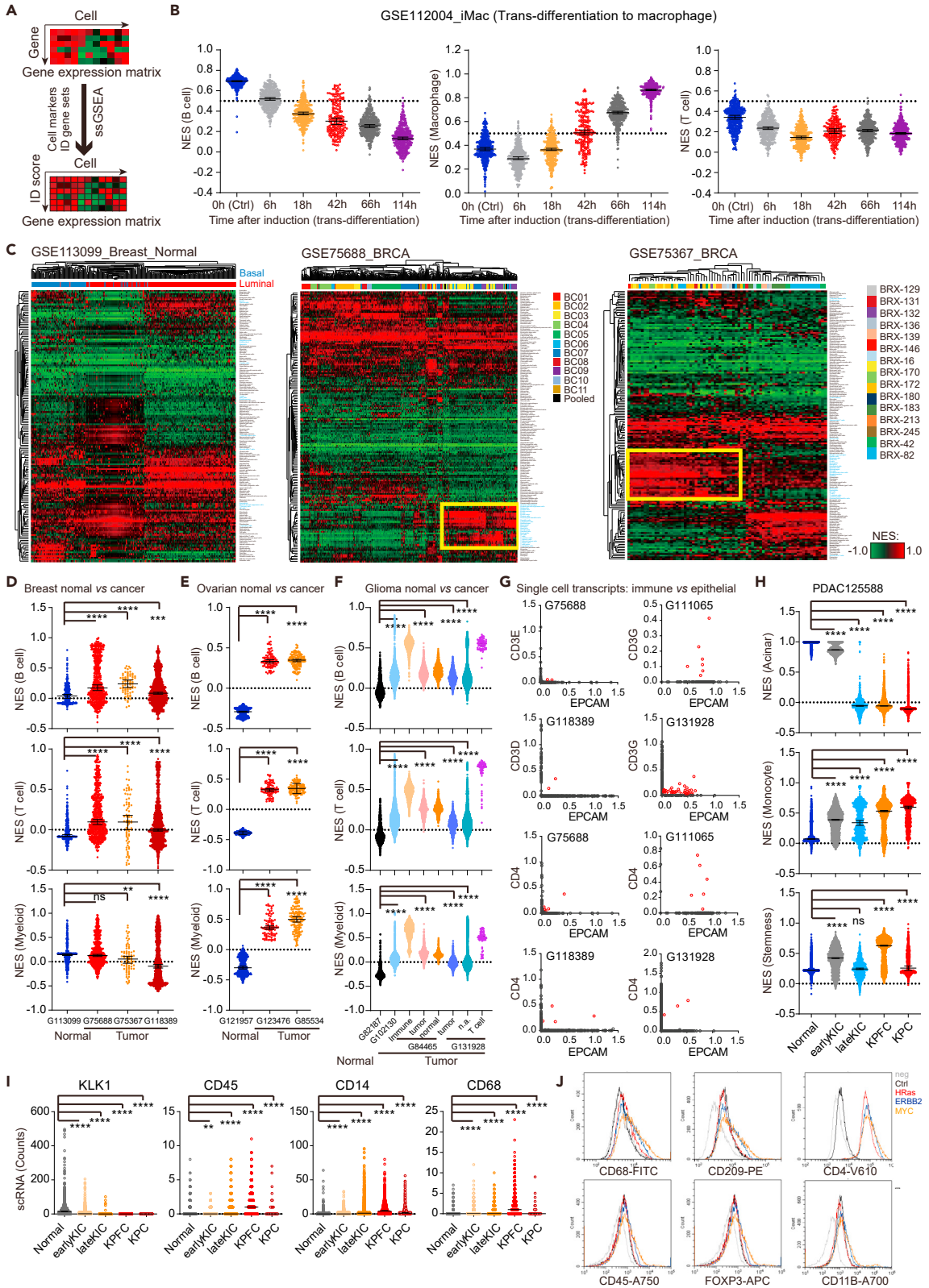
A
Cell
Gene
Gene expression matrix
Cell markers
ID gene sets
ssGSEA
Cell
ID score
Gene expression matrix
B
GSE112004_iMac (Trans-differentiation to macrophage)
NES (B cell)
NES (Macrophage)
NES (T cell)
0h (Ctrl) 6h 18h 42h 66h 114h
Time after induction (trans-differentiation)
C
GSE113099_Breast_Normal
GSE75688_BRCA
GSE75367_BRCA
Basal
Luminal
BC01
BC02
BC03
BC04
BC05
BC06
BC07
BC08
BC09
BC10
BC11
Pooled
BRX-129
BRX-131
BRX-132
BRX-136
BRX-139
BRX-146
BRX-16
BRX-170
BRX-172
BRX-180
BRX-183
BRX-213
BRX-245
BRX-42
BRX-82
NES:
-1.0
1.0
D
Breast nomal vs cancer
NES (B cell)
NES (T cell)
NES (Myeloid)
G113099 G75688 G75367 G118389
Normal
Tumor
E
Ovarian nomal vs cancer
G121957 G123476 G85534
F
Glioma nomal vs cancer
G82187 G112130 Immune tumor normal tumor n.a. T cell
G84465 G131928
G
Single cell transcripts: immune vs epithelial
G75688
G111065
G118389
G131928
CD3E
CD3G
CD3D
CD4
EPCAM
H
PDAC125588
NES (Acinar)
NES (Monocyte)
NES (Stemness)
Normal earlyKIC lateKIC KPFC KPC
I
KLK1
CD45
CD14
CD68
scRNA (Counts)
J
CD68-FITC
CD209-PE
CD4-V610
CD45-A750
FOXP3-APC
CD11B-A700
neg
Ctrl
HRas
ERBB2
MYC

Figure 1. Single-cell immune-like reprogramming in cancer cells

(A) Illustration of single-cell transcription-based deconvolution of cellular differentiation genes by the single sample GSEA (ssGSEA).

(B) The dynamics of single-cell ssGSEA scores in cells *trans*-differentiating from B cells to macrophages (GSE112004). The B cell (left), macrophage (middle) and T cell (right) normalized scores are present at different time points (hours, h) after induction.

(C) Normalized ssGSEA scores of breast epithelial cells (left panel) and breast cancer cells. Color bars indicate cell types of different origin.

(D–F) Immune cell genes, including B cell (upper panel), T cell (middle panel), and myeloid (lower panel) genes between normal and cancer cells in breast cancer (D), ovarian cancer (E), and glioma (F). Normalized ssGSEA scores of individual cancer cells compared with normal cells from the same tissues. Cells in GSE84465 and GSE131928 were split into different subsets according to the predefined groups in the dataset.

(G) Plots showing the normalized expression of immune genes (CD4, CD3D, CD3E, and CD3G) and epithelial marker (EPCAM) in individual cells among different datasets. The expression values were normalized according to GAPDH levels. Red dots indicate cells expressing both immune and epithelial marker genes.

(H) Plots showing the ssGSEA scores of acinar, stemness, and monocyte in different stages of pancreatic ductal adenocarcinoma (PDAC) development dataset (GSE125588).

(I) Expression of acinar (KLK1) and immune cell (CD45, CD14, and CD68) markers in PDAC dataset.

(J) Flow cytometry analysis of immune cell markers in MCF-10A or MCF10A cells expressing doxycycline (Dox) inducible expression of ERBB2, $HRAS^{G12V}$ and MYC. Cells were treated with Dox for 8 days before analysis. Error bars in (B), (C–F), and (G and H) represent median and 95% CI. p values, two-sided Mann Whitney Wilcoxon test (ns, not significant; **, $p < 0.01$; ***, $p < 0.001$; ****, and $p < 0.0001$). See also Figure S1.

myeloid derived suppressor cells are tumor-promoting (Havel et al., 2019). In contrast, macrophages, neutrophils, and dendritic cells could either promote or suppress tumor development in a context dependent manner (Szczerba et al., 2019; Wculek et al., 2020). Indeed, in certain cases, immune processes are hijacked by cancer to drive cancer progression (Szczerba et al., 2019). Therefore, it is essential to clarify the specific roles of different immune processes in the tumor microenvironment. However, the cellular network in the immune microenvironment remains poorly characterized.

Here, based on scRNA-seq datasets and oncogenic transformation models, we uncover that an immune-like transcriptional program is a distinct feature acquired in oncogenic transformation. The immune mimicry is consistently observed in a variety of cancer cells, contributing to the inconsistencies of immune gene signature-based analyses. An optimized immune response signature (oIRS) reduces this transcriptional noise by improving immune cell specificity, and redefining prognostic association of immune processes. Moreover, immune networks underlying oIRS point to antigen presentation, NK cell killing, and T cell signaling as the processes consistently associated with favorable clinical outcomes, indicating favorable response to immunotherapy in patients.

RESULTS

Immune-like transcriptional reprogramming is a distinct cancer hallmark

To determine how the normal differentiation programs are deregulated in individual cancer cells, we developed an approach to evaluate the single-cell expression of cellular differentiation genes by single sample gene set enrichment analysis (ssGSEA) (Barbie et al., 2009) in single-cell RNA-seq datasets. The enrichment scores of 172 distinct cell marker gene sets, representing the levels of marker gene expression, were used to evaluate the expression of cellular differentiation genes in individual cells (Figure 1A). The ssGSEA approach was validated by its ability to demonstrate a progressive change of differentiation programs during the *trans*-differentiation from B cells to macrophages (GSE112004 (Francesconi et al., 2019), Figure 1B). Notably, single-cell expression of cellular differentiation genes in breast cancer indicated an elevated immune activity in cancer cells (GSE75688 (Chung et al., 2017) and GSE75367 (Jordan et al., 2016)) compared with normal breast epithelia (GSE113099 (Nguyen et al., 2018), Figure 1C). Consistently, active immune signatures in single cancer cells were confirmed in colon cancer and glioblastoma (GSE81861 (Li et al., 2017) and GSE131928 (Neftel et al., 2019), Figures S1A and S1B).

To characterize the immune-like transcriptional features of single cancer cells, we examined the expression of cellular differentiation genes in malignant and normal cells from a variety of tissues. Interestingly, immune-like transcripts were elevated in the malignant cells compared with their normal counterparts. Specifically, the enrichment scores of B cell, T cell and myeloid cell signatures were higher in breast cancer compared to those in normal epithelial cells (GSE113099, GSE75688, GSE75367 and GSE118389 (Karaayvaz et al., 2018), Figure 1D). Enrichments of immune cell signatures were confirmed in single cancer cells from ovarian cancer (GSE121957 (Vuong et al., 2018), GSE123476 (Winterhoff et al., 2017) and GSE85534 (Guillaumet-Adkins et al., 2017), Figure 1E) and glioblastoma (GSE82187 (Gokce et al., 2016), GSE102130 (Filbin et al., 2018), GSE84465 (Darmanis et al., 2017) and GSE131928, Figure 1F). Moreover, B cell, T cell, and

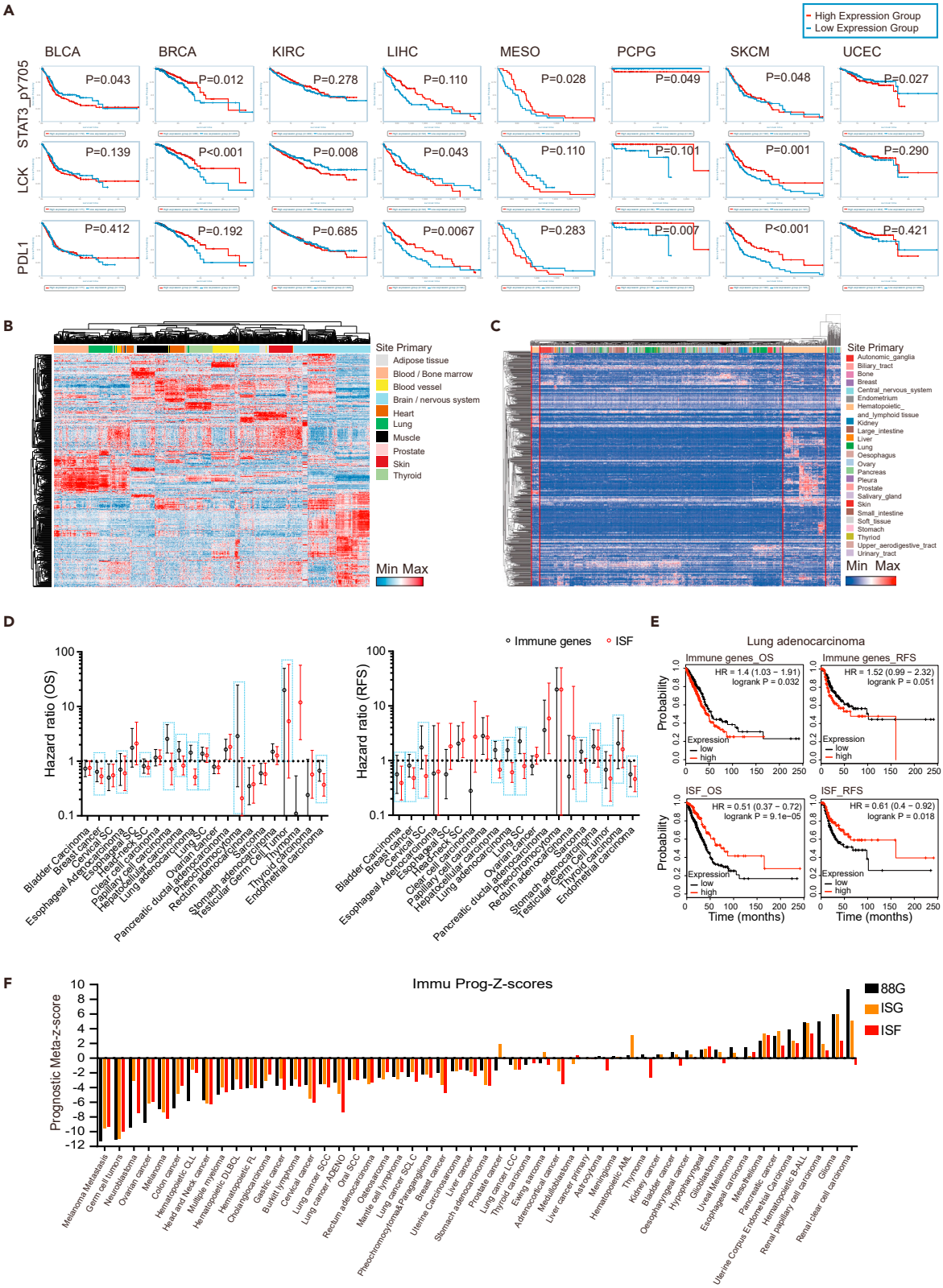
A
High Expression Group
Low Expression Group
BLCA
BRCA
KIRC
LIHC
MESO
PCPG
SKCM
UCEC
STAT3_pY705
LCK
PDL1
P=0.043
P=0.012
P=0.278
P=0.110
P=0.028
P=0.049
P=0.048
P=0.027
P=0.139
P<0.001
P=0.008
P=0.043
P=0.110
P=0.101
P=0.001
P=0.290
P=0.412
P=0.192
P=0.685
P=0.0067
P=0.283
P=0.007
P<0.001
P=0.421
B
Site Primary
Adipose tissue
Blood / Bone marrow
Blood vessel
Brain / nervous system
Heart
Lung
Muscle
Prostate
Skin
Thyroid
Min Max
C
Site Primary
Autonomic_ganglia
Biliary_tract
Bone
Breast
Central_nervous_system
Endometrium
Hematopoietic_and_lymphoid tissue
Kidney
Large_intestine
Liver
Lung
Oesophagus
Ovary
Pancreas
Pleura
Prostate
Salivary_gland
Skin
Small_intestine
Soft_tissue
Stomach
Thyriod
Upper_aerodigestive_tract
Urinary_tract
Min Max
D
Immune genes
ISF
Hazard ratio (OS)
Hazard ratio (RFS)
E
Lung adenocarcinoma
Immune genes_OS
HR = 1.4 (1.03 − 1.91)
logrank P = 0.032
Immune genes_RFS
HR = 1.52 (0.99 − 2.32)
logrank P = 0.051
ISF_OS
HR = 0.51 (0.37 − 0.72)
logrank P = 9.1e−05
ISF_RFS
HR = 0.61 (0.4 − 0.92)
logrank P = 0.018
Probability
Expression
low
high
Time (months)
F
Immu Prog-Z-scores
Prognostic Meta-z-score
88G
ISG
ISF

Figure 2. Cancer-derived transcriptional noise contributes to inconsistent immune prognoses

(A) Kaplan Meier analysis of patients with low (blue curve) and high (red curve) expression of STAT3_ pY05, LCK and PDL1 in the TCPA datasets. p values were determined by log rank test.

(B) Hierarchical clustering of leukocyte gene signature matrix (CIBERSORT) genes in the GTEX dataset. Column sidebar represents tissue origin.

(C) Hierarchical clustering of CIBERSORT genes in the CCLE dataset. Red line indicates hematopoietic and lymphoid derived cell lines. Column sidebar represents the tissue origin of cell lines.

(D) Hazard ratio based on the OS and RFS data in all cancers. Hazard ratio (95% CI) for immune gene (upper panel) or ISF (lower panel) gene signature in the Kaplan Meier plotter datasets. Cancers with lower hazard ratio (left y axis) were marked with blue boxes. p values (right y axis) were determined by log rank test.

(E) Kaplan Meier analysis of patients with low (black curve) and high (red curve) expression of immune gene (upper panel) or ISF (lower panel) gene signature in the Kaplan Meier plotter datasets. p values, log rank test.

(F) The prognostic meta-*z* sores of immune gene signatures among different cancer types. Meta-*z* scores were calculated by unweighted prognostic *z* scores of individual genes in each signature. Black bars, immune genes; orange bars, optimized immune response signature (oIRS, 32 genes); and red bars, immune-specific favorable gene set (ISF,19 genes). See also Figure S2

myeloid signatures were enriched in a number of cancer types, including lung cancer (GSE136580 (Ouadah et al., 2019) GSE69405 (Kim et al., 2015)), kidney cancer (GSE119531 (Wu et al., 2019) and GSE73121 (Kim et al., 2016)), pancreatic cancer (GSE85241 (Muraro et al., 2016) and GSE129455 (Elyada et al., 2019)), glioma (GSE82187 and GSE89567 (Venteicher et al., 2017)), and oligodendroglioma (GSE70630 (Tirosh et al., 2016), Figure S1C). The ssGSEA scores of immune signatures in cancer cells were higher than in normal cells, but lower than those in immune cells (with a median ssGSEA score of 0.7–0.8 in Figures 1B and 1F), indicating a partial gain of immune gene expression in cancer (Figures 1B and 1D–F). Indeed, specific immune cell markers, including CD3D, CD3E, CD3G, and CD4, were expressed in a proportion of individual cancer cells (Figure 1G). These findings suggest that immune-like transcriptional reprogramming is a distinct hallmark of cancer cells.

We next determined whether immune-like transcriptional reprogramming occurs in the process of malignant transformation. To this end, scRNA-seq of a pancreatic ductal adenocarcinoma development model, including normal pancreatic, early KIC ($Kras^{LSL-G12D/+}Ink4a^{fl/fl}Ptf1a^{Cre/+}$), late KIC, KPFC ($Kras^{LSL-G12D/+}Trp53^{fl/fl}Pdx1^{Cre/+}$), and KPC ($Kras^{LSL-G12D/+}Trp53^{LSL-R172H/+}Pdx1^{Cre/+}$) cells GSE125588 (Hosein et al., 2019) was reanalyzed. Indeed, monocyte and stemness signatures were progressively increased, and the acinar signature was decreased in the process of tumorigenesis, indicating the plasticity and immune mimicry in pancreatic cancer development (Figure 1H). The enrichment scores were further verified by individual transcripts, including KLK1, CD45 and CD14 in the dataset (Figures 1I and S1D). Indeed, the *t*-SNE clustering identified a distinct early KIC cell cluster with both moderate acinar and monocyte signature expression, and another cluster with ductal and monocyte signatures, confirming the immune mimicry in transformed epithelial cells (Figure S1E). Consistently, a cluster of luminal epithelial cells in p53/BRCA1 breast tumor (Wang et al., 2019) showed increased expression of immune transcripts (Figure S1F). To gain experimental evidence of immune mimicry in malignant transformation, we analyzed the expression of immune cell markers in MCF-10A cells undergoing oncogene-induced transformation (Figure S1G). In agreement, individual oncogene induced cells showed increased expression of immune cell markers, including CD45, CD68, and CD4, thus collaborating the concept of immune mimicry in cancer (Figure 1J).

oIRS refines tumor immune infiltration analysis

The immune transcripts in cancer cells may be considered as tumor infiltrating immune cells in the conventional tumor mass profile-based immune infiltration analysis, which is currently used to assess the immune infiltrating status in cancer (Gentles et al., 2015; He et al., 2019). To test the hypothesis, the prognostic pattern in the Cancer Proteome Atlas (TCPA) database (Li et al., 2013) was analyzed. Interestingly, activated (STAT3_pY705) STAT3, a core transcription factor in immune cell signaling (Yu et al., 2014), was associated with favorable prognosis in several cancers, but not bladder carcinoma, pheochromocytoma-paraganglioma, and uterine corpus endometrial carcinoma (Figure 2A, upper panel). LCK, a critical player in T-cell antigen receptor (TCR)-linked signaling, was associated with adverse prognosis in kidney and liver cancer (Figure 2A, middle panel). The immune checkpoint ligand PD-L1, a core immunosuppressive molecule, displayed variable prognoses in different cancer types (Figure 2A, lower panel). Similar prognostic patterns were found in pheochromocytoma-paraganglioma and mesothelioma, confirming the cancer type dependent prognostic pattern of immune genes (Figure 2A). Interestingly, the prognostic pattern of PD-L1 was similar in breast, ovarian, lung, and gastric patients with different treatment status, suggesting

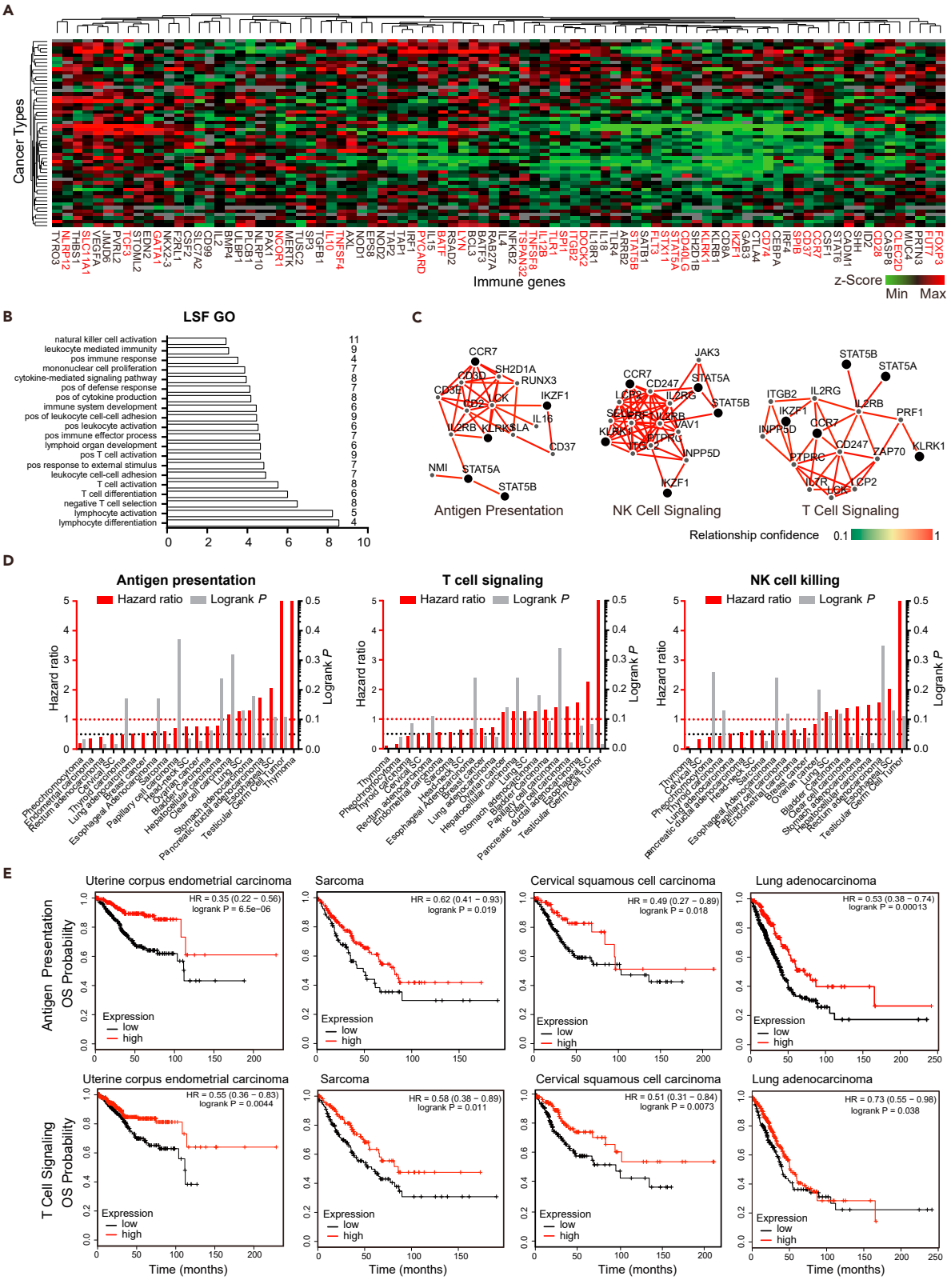
A
Cancer Types
Immune genes
z-Score
Min Max
B
LSF GO
natural killer cell activation
leukocyte mediated immunity
pos immune response
mononuclear cell proliferation
cytokine-mediated signaling pathway
pos of defense response
pos of cytokine production
immune system development
pos of leukocyte cell-cell adhesion
pos leukocyte activation
pos immune effector process
lymphoid organ development
pos T cell activation
pos response to external stimulus
leukocyte cell-cell adhesion
T cell activation
T cell differentiation
negative T cell selection
lymphocyte activation
lymphocyte differentiation
C
Antigen Presentation
NK Cell Signaling
T Cell Signaling
Relationship confidence
D
Antigen presentation
T cell signaling
NK cell killing
Hazard ratio
Logrank P
E
Uterine corpus endometrial carcinoma
Sarcoma
Cervical squamous cell carcinoma
Lung adenocarcinoma
Antigen Presentation OS Probability
T Cell Signaling OS Probability
Expression
low
high
Time (months)

Figure 3. Favorable prognoses of core anti-tumor immune processes

(A) Hierarchical clustering of immune genes according to PRECOG z-scores in 52 tumor cohorts.

(B) Histogram showing the 16 favorable ISF genes enriched in Gene Ontology biological processes. The numbers of enriched genes in the GO term are listed on the right. p values were EASE scores (modified Fisher Exact p value) provided in the DAVID database.

(C) Networks of the top 5 favorable ISF genes (CCR7, STAT5B, IKZF1, STAT5A, and KLRK1) in the ImmuNet database. The enriched network for antigen processing and presentation is shown on the left, the natural killer cell mediated cytotoxicity network is given in the middle, and the T cell signaling is shown on the right. Sidebar: relationship confidence (0.1–1.0).

(D) Hazard ratio based on the OS data in all cancers. Hazard ratio for antigen presentation (left panel), T cell signaling (middle panel) and NK cell mediated cytotoxicity (right panel) gene signatures in the Kaplan Meier plotter datasets was shown. Cancers with lower hazard ratio (left y axis) were marked with blue boxes. p values (right y axis) were determined by log rank test.

(E) Kaplan Meier analysis of overall survival in patients with low (black curve) and high (red curve) expression gene signatures. Antigen presentation (upper panel) and T cell signaling (lower panel) gene signatures were assessed in the Kaplan Meier plotter datasets. p values, log rank test. See also Figure S3.

no direct link between conventional treatment status (chemotherapy/endocrine therapy) and the prognostic pattern of immune markers (Figure S2A). In addition, gene expression in immunotherapy responding and non-responding patients indicated a weak correlation between these immune transcripts and immunotherapy response (Figure S2B). These results indicate a tumor intrinsic mechanism that contributes to the inconsistent prognostic pattern of immune genes in different cancers.

We next determined whether the immune genes expressed in certain cancer cells contribute to the inconsistent prognoses of immune genes. The CIBERSORT 547 immune gene signatures (Newman et al., 2015) which represent immune cell subsets have been applied in the analysis of immune activity in tumor specimens (Gentles et al., 2015). Hierarchical clustering of the signature genes in normal tissues (GTEX dataset) showed that they were enriched in blood/bone marrow, albeit widely expressed in many other tissues (Figure 2B). Moreover, cancer cells from various tissues, shown in the cancer cell line encyclopedia (CCLE) dataset (Barretina et al., 2012), expressed considerable levels of the CIBERSORT immune genes (Figure 2C). Indeed, the expression levels of the CIBERSORT genes in CCLE confirmed a significant enrichment of immune genes in hematopoietic and lymphoid derived cell lines, yet a considerable number of genes were detected in non-hematopoietic cancer cells. These results confirm the existence of cancer cell-derived immune transcripts, which may confound conventional immune gene signature-based analysis.

Next, we determined whether reducing cancer cell-derived transcripts improve the prognostic consistencies of immune gene signatures. Specifically, gene signatures of functional immune processes in dendritic cells, macrophages, CD8 T cells, B cells, and NK cells were collected from the Gene Expression Commons database. According to the transcriptional profiles from the CCLE dataset, we identified a 32-gene optimized immune response signature (oIRS), 19 of which showed favorable prognostic scores in more than 50% of the cancer cohorts (He et al., 2019) (immune specific favorable genes, ISF). The prognostic value of the ISF gene signature was compared with that of the parental immune gene signature. In agreement with our hypothesis, the hazard ratio in 41 datasets indicated that ISF showed better prognoses than the parental signature in 21 of the 41 datasets (Figure 2D). For instance, favorable prognosis of ISF was found in lung adenocarcinoma, pheochromocytoma-paraganglioma, and hepatocellular carcinoma, where the parental immune signature indicated adverse prognosis (Figures 2D and 2E). Indeed, ISF performed better in distinguishing patient subsets, indicating better prognoses in other cohorts including breast cancer, endometrial carcinoma, and bladder carcinoma (Figures S2C and S2D). Furthermore, the pan-cancer prognostic meta-*z* scores of ISF were lower compared to those of parental immune genes, confirming a better prognostic pattern after reducing cancer-derived immune transcripts (Figure 2F).

ISF points to core tumor suppressive immune processes

Our results led us to speculate that the biological processes underlying the ISF signature, which consistently indicates favorable prognosis in cancer, might reveal the conserved anti-tumor immune processes. To profile the prognoses of functional immune genes, we examined the prognostic *z* scores of functional immune genes in 52 cancer types from the PreCOG and TCGA cohorts (Figure 3A). The results showed 16 genes were associated with favorable prognosis in more than 60% of the cancer types (z score < 0, Figure 3A). Gene Ontology (GO) analysis was applied to determine whether there are immune processes involved. The 16 ISF genes were enriched in immune processes, including natural killer cell activation, leukocyte mediated immunity and positive immune response (Figure 3B). To further determine the immune signaling networks associated with the immune specific genes with favorable prognosis, we examined the top 5 favorable genes (CCR7, IKZF1, KLRK1, SAT5B, and SAT5A) in the ImmuNet database (Gorenshteyn

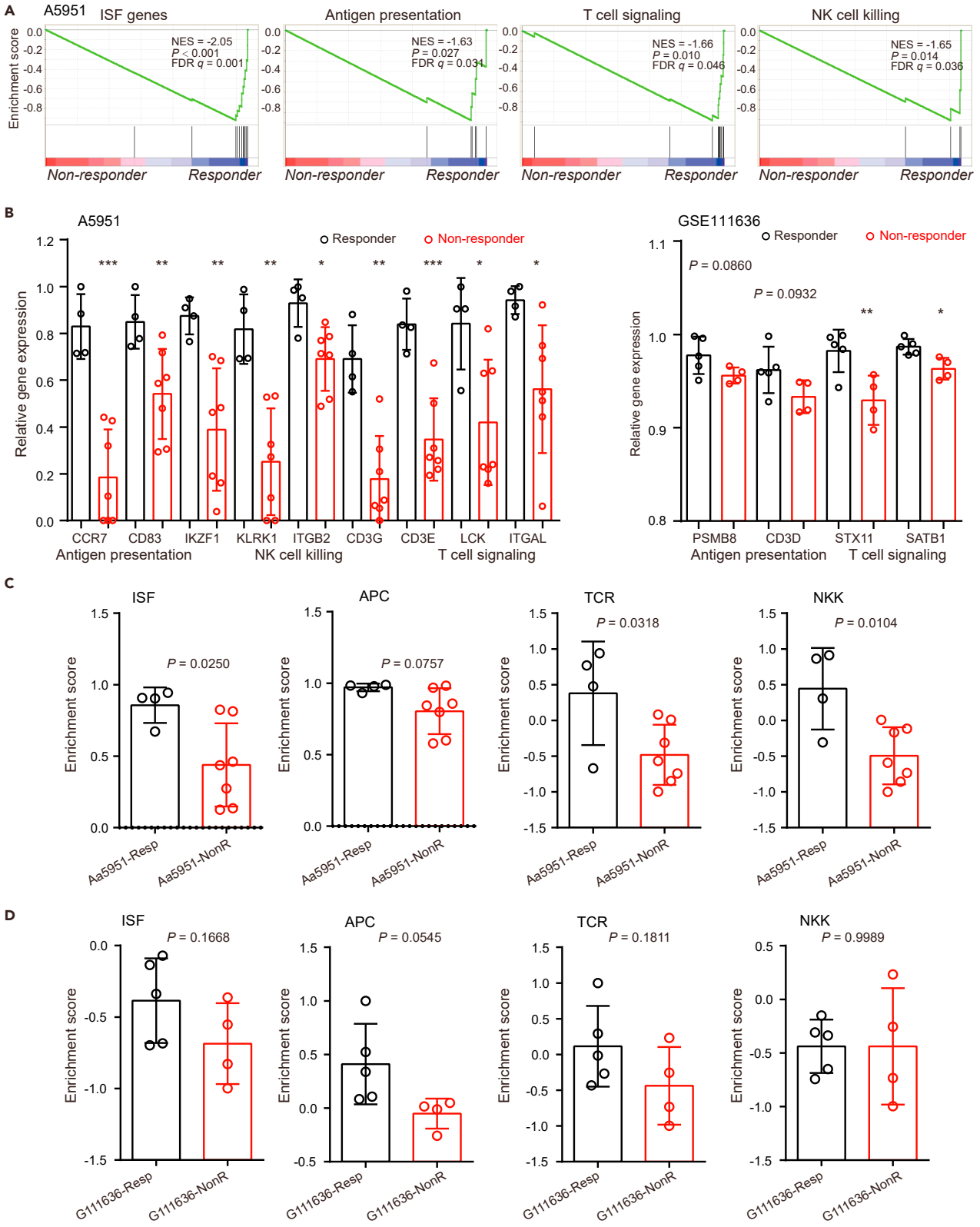
A
A5951
ISF genes
Antigen presentation
T cell signaling
NK cell killing
Enrichment score
NES = -2.05
P < 0.001
FDR q = 0.001
NES = -1.63
P = 0.027
FDR q = 0.031
NES = -1.66
P = 0.010
FDR q = 0.046
NES = -1.65
P = 0.014
FDR q = 0.036
Non-responder
Responder
B
A5951
Responder
Non-responder
Relative gene expression
CCR7
CD83
IKZF1
KLRK1
ITGB2
CD3G
CD3E
LCK
ITGAL
Antigen presentation
NK cell killing
T cell signaling
GSE111636
P = 0.0860
P = 0.0932
PSMB8
CD3D
STX11
SATB1
C
ISF
APC
TCR
NKK
P = 0.0250
P = 0.0757
P = 0.0318
P = 0.0104
Aa5951-Resp
Aa5951-NonR
D
P = 0.1668
P = 0.0545
P = 0.1811
P = 0.9989
G111636-Resp
G111636-NonR

Figure 4. Anti-tumor immune processes correlate with immunotherapy response

(A) Representative enrichment plots for ISF, antigen presentation, T cell signaling and NK cell killing gene sets. Normalized enrichment scores (NES), false discovery rate (FDR) and p values were determined by GSEA in gene expression profiles of responders and non-responder in the in Aa5951 dataset.

(B) Histogram showing the expression of antigen presentation, T cell signaling and NK cell killing genes in immunotherapy responder or non-responder patients from Aa5951 (left panel) and GSE111636 (right panel) datasets.

(C and D) Enrichment scores of ISF, antigen presentation cells (APC), T cell receptor signaling (TCR) and NK cell killing (NKK) in immunotherapy responders (Resp) or non-responders (NonR). Enrichment scores were determined by single-sample GSEA in Aa5951 (C) and GSE111636 (D). Data in (B–D) are represented as mean ± SD. p values, two-tailed Student's *t* test (*, $p < 0.05$; **, $p < 0.01$; ***, $p < 0.001$).

et al., 2015). Of the nine immune networks analyzed, the processes Antigen Processing and Presentation, NK Cell Mediated Cytotoxicity and T cell signaling were significantly enriched (Figure 3C).

To validate whether these immune processes indicate favorable outcome, we analyzed the specific representative genes of these immune processes in the Kaplan-Meier plotter database (Gyorffy et al., 2010, 2013). The T cell signaling (LCK, CD247, ITGB2, TNFSF8, and DOCK2), Antigen presentation (CD74, CD37, CCR7, CD40LG, and FLT3) and NK cell cytotoxicity (ARBB2, SH2D1B, IKZF1, KLRB1, and KLRK1) gene signatures all indicated favorable clinical outcomes in patients. Thus, both overall survival (OS) and disease-free survival (DFS) were longer in patients with higher expression levels of these signatures across multiple cancer types (Figures 3D and 3E, and S3). Thus, we characterized a set of immune-specific favorable immune genes that present core tumor suppressive immune processes in cancer.

Core immune processes indicate effective immunotherapy

Next, we sought to determine whether the immune processes identified by ISF are associated with clinical response to immunotherapy in cancer. To this end, we inspected datasets with both transcriptional profiles of pre-treated tumors and patients' responses to immunotherapies. Patients were classified as responder and non-responder subsets according to their sensitivity to immunotherapy. A gene set enrichment analysis (GSEA) (Subramanian et al., 2005) was performed in immunotherapy responder and non-responder patients based on their transcriptional profiles. Indeed, the ISF gene set, antigen presentation, T cell signaling and NK cell killing gene sets were enriched in the responder subset (Aa5951 (Miao et al., 2018), Figure 4A, $p < 0.05$, FDR < 0.05, NES = −2.05, −1.63, −1.66, and −1.65, respectively). Consistently, the expression of antigen presentation (APC), T cell signaling and NK cell killing genes were higher in immunotherapeutic responders than non-responders from both Aa5951 (left panel) and GSE111636 (Segovia et al., 2019) (right panel) datasets (Figure 4B). Moreover, higher ssGSEA scores of these gene sets, which indicate higher activities of the anti-tumor immune processes, were confirmed in the responder patients (Figures 4C and 4D). Altogether, these results provide strong evidence to support that anti-tumor immune processes underlying favorable prognostic processes are associated with response to immunotherapy.

APC is an independent breast cancer prognostic factor

Antigen processing and presentation is essential for adaptive immune cell activation. To confirm the clinical association of antigen presentation genes, we selected lymphocyte specific antigen presentation genes based on the gene expression patterns in cancer cell lines (CCLE dataset, Figure 5A). A group of genes, including CD40LG, CD83, CCR7, CD37, and GATA1, were confirmed as favorable prognostic genes according to the PRECOG dataset (Figure 5B). To validate the clinical association of individual genes, we determined the prognoses of each gene in different tumor types using the Kaplan Meier database. High expression of CD40LG, CCR7, and CD37 were consistently associated with favorable clinical outcomes in a panel of cancers, including breast, cervical, head-neck, lung adenocarcinoma, sarcoma and endometrial carcinoma, and GATA1 showed similar prognostic pattern in cancers except endometrial carcinoma (Figures 5C, S4A, and S4B). CD83, a member of the immunoglobulin superfamily that are expressed on the surface of activated dendric cells and other antigen presentation cells (Li et al., 2019), correlates with favorable prognosis in several cancer types (Figures 5D, 5E, S4C, and S4D).

To further validate these findings, we studied the expression of CD83 in 366 breast cancer specimens. Tumor-infiltrating CD83 positive ($CD83^+$) cells were observed in a subset of breast cancer specimens (Figure 5F). The antigen processing/presentation status in patients were determined by counting the infiltrating $CD83^+$ cells in each patient. In keeping with the hypothesis, patients with high $CD83^+$ cell density exhibited better OS and DFS in breast cancer ($P = 0.003$ and $P = 0.018$, respectively, Figure 5G). Moreover, Cox regression analysis showed that $CD83^+$ cell density was a significant factor in determining both OS and

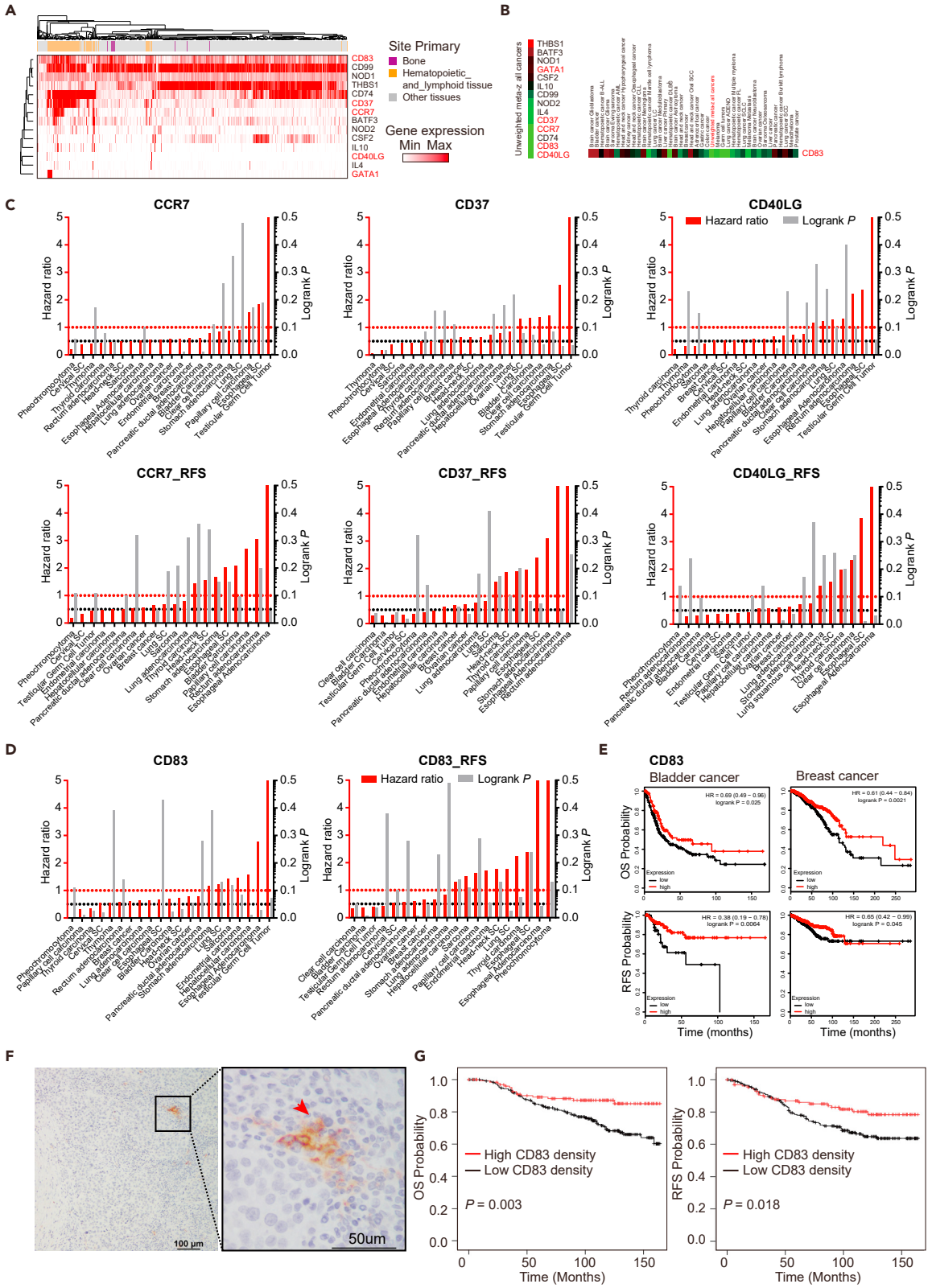
A
Site Primary
Bone
Hematopoietic_ and_lymphoid tissue
Other tissues
Gene expression
Min Max
CD83
CD99
NOD1
THBS1
CD74
CD37
CCR7
BATF3
NOD2
CSF2
IL10
CD40LG
IL4
GATA1
B
Unweighted meta-z all cancers
THBS1
BATF3
NOD1
GATA1
CSF2
IL10
CD99
NOD2
IL4
CD37
CCR7
CD74
CD83
CD40LG
CD83
C
CCR7
CD37
CD40LG
Hazard ratio
Logrank P
CCR7_RFS
CD37_RFS
CD40LG_RFS
D
CD83
CD83_RFS
Hazard ratio
Logrank P
E
CD83
Bladder cancer
Breast cancer
OS Probability
RFS Probability
Expression
low
high
Time (months)
F
100 μm
50um
G
High CD83 density
Low CD83 density
P = 0.003
P = 0.018
OS Probability
RFS Probability
Time (Months)

Figure 5. Antigen presentation predicts favorable prognosis in breast cancer

(A) Hierarchical clustering of antigen presentation genes according to their expression in cancer cell lines (CCLE dataset). Genes showing lymphocyte specific expression patterns were labeled in red.

(B) The pan-cancer PRECOG z-scores of antigen presentation genes (left panel). PRECOG z-score of CD83 in different cancer types (right panel).

(C) Hazard ratio based on the OS (upper panel) and RFS (lower panel) data in all cancers. Hazard ratio for CCR7, CD37 and CD40LG in the Kaplan Meier plotter datasets was shown. p values (right y axis) were determined by log rank test.

(D) Hazard ratio of CD83 based on the OS (left panel) and RFS (right panel) data in all cancers. p values (right y axis) were determined by log rank test.

(E) Kaplan Meier analysis of relapse free survival (RFS) in patients with low (black curve) and high (red curve) expression of CD83 in the Kaplan Meier plotter datasets. p values, log rank test.

(F) Representative IHC staining of CD83 in breast cancer specimens. Arrow indicates CD83 + cells. Scale bar represents 50μm.

(G) Kaplan Meier curves of estimated overall survival (OS, left panel) and disease-free survival (DFS, right panel) of breast cancer patients with low (<1 per view of field, n = 238) and high (≥1 per view of field, n = 128) CD83 + cell density ($p < 0.01$ by the log rank test). See also Figure S4.

DFS in breast cancer ($P = 0.003$ and 0.019, respectively, Tables 1 and 2). Indeed, multivariate Cox regression analysis suggested that $CD83^+$ cell density was an independent factor in determining both OS and DFS in breast cancer ($P = 0.001$ and 0.012, respectively, Tables 1 and 2). In contrast to the other factors, tumor size and distant metastasis were better correlated with $CD83^+$ cell density ($P = 0.053$ and 0.181, respectively, Table 3). This data provided experimental evidence that antigen presentation is an independent prognosis factor indicative of favorable outcome for breast cancer.

DISCUSSION

Plasticity of cancer cells, characterized by the differentiation statuses that are transcriptionally reprogrammed to mimic differentiation programs of normal cells is increasingly appreciated. Of note, immune mimicry programs that facilitate immune invasion (Gangoso et al., 2021) pose a challenge to the current landscape of tumor microenvironment that are based primarily on tumor mass profiling. We focused on this issue by providing evidence that single cancer cells show immune mimicry in multiple cancer types and tumorigenesis models. These findings, together with those from a previous report (Nishida et al., 2020), indicate that cancer cells might hijack immune processes to remodel the tumor microenvironment. Notably, immune mimicry provides a refined view of immune-infiltration analyses based on the tumor mass profiles. Current "immune-infiltrating cells" based on tumor mass profiles does not exclude the "immune mimicry transcripts" in cancer cells (Gentles et al., 2015; Newman et al., 2015). Thus, deconvolution of the "immune mimicry" programs in cancer cells could provide a refined view of the immune-infiltrating landscape.

The optimized immune response signature (oIRS), which excludes "immune mimicry transcripts" from immune gene signatures, offers a more favorable prognostic value. For instance, improved specificity confers favorable prognosis in breast cancer and lung adenocarcinoma, which exhibit adverse immune prognosis before oIRS specification. The finding confirms a role of immune mimicry in signature-based tumor

Table 1. Cox regression analysis of OS in the breast cancer cohort (n = 366)

	Univariate		Multivariate	
Parameters	*P*	HR	95%CI	p value
Age (>50)	0.262			
Premenopausis	0.406			
Tumor size (>2cm)	0.002	1.384	0.797–2.403	0.248
Node status (positive)	0.002	1.066	0.613–1.851	0.822
Tumor grade (III)	0.933			
Stage (III)	<0.001	4.309	2.713–6.846	<0.001[a]
ER (positive)	0.229			
PR (positive)	0.251			
HER2 (positive)	0.108			
Ki67 (positive)	0.061			
CD83 (positive)	0.003	0.409	0.237–0.707	0.001[a]

[a]$p < 0.05$ in both Univariate and Multivariate analyses.

Table 2. Cox regression analysis of DFS in the breast cancer cohort (n = 366)

	Univariate		Multivariate	
Parameters	*P*	HR	95%CI	p value
Age (>50)	0.706			
Premenopause	0.395			
Tumor size (>2cm)	0.001	1.204	0.631–2.300	0.573
Node status (positive)	<0.001	1.802	0.888–3.657	0.103
Tumor grade (III)	0.142			
Stage (III)	<0.001	2.438	1.330–4.469	0.004[a]
ER (positive)	0.976			
PR (positive)	0.621			
HER2 (positive)	0.031	1.115	0.630–1.973	0.709
Ki67 (positive)	0.013	0.509	0.229–1.130	0.097
CD83 (positive)	0.019	0.449	0.240–0.841	0.012[a]

[a]$p < 0.05$ in both Univariate and Multivariate analyses.

immune-infiltration analyses. Indeed, immune gene signatures for the prevailing prognostic analysis (CIBERSORT) (Gentles et al., 2015; Newman et al., 2015) is expressed in a substantial proportion of normal tissues and tumor cell lines from different tissues. By characterizing immune specific genes, our approach provides a precise insight into the prognostic significance of the immune infiltration status in cancer. Integration of the refined immune signaling networks reveals that biological processes in antigen processing, NK cell killing and T cell signaling predict favorable outcomes in multiple cancer cohorts.

Immune processes are thought to be "double edged sword" in cancer. Specifying anti-tumor or tumor-promoting immune processes is thus critical for a better understanding of tumor-immune interactions and for predicting effective immunotherapy. Recently, integrative analyses of tumor transcriptional profiles have established that immune processes are associated with favorable outcome in a number of cancers (Gentles et al., 2015; He et al., 2019), in agreement with the favorable prognosis of immunoscore (Mlecnik et al., 2016) and successes of immunotherapy in a proportion of patients (Hodi et al., 2010; Postow et al., 2015). However, these studies consistently find that immune processes are not always associated with favorable clinical outcomes. Indeed, higher immune activity correlates with worse prognosis in a notable number of patient cohorts. The consistent prognostic inconsistencies of immune processes in different cancer contexts indicate that unknown prognostic factors remain to be defined. The oIRS in this study provides an improved prognostic pattern of immune processes by specifying tumor infiltrating immune status.

These favorable processes also serve as candidate therapeutic targets and biomarkers for predicting clinical response to immunotherapies. We have also looked into independent patient cohorts treated with immunotherapy. In agreement with previous reports (Maier et al., 2020), higher activity of antigen processing, NK cell killing, and T cell signaling, indicated by high related immune gene expression, are associated with favorable response to immunotherapy. Through analyzing $CD83^+$ mature dendritic cell infiltration in breast tumor tissues, we have experimentally validated antigen presentation as a favorable prognostic factor. In addition, experimental data further confirm that CD83 is a significant factor in determining both overall survival and disease-free survival in breast cancer. These findings, together with previous reports that tumor infiltrating $CD83^+$ dendritic cell is a favorable prognostic factor (Iwamoto et al., 2003; McMullen et al., 2010), underline the important role of $CD83^+$ dendritic cell in shaping the tumor-suppressive immune microenvironment. In summary, these findings establish that immune-like transcriptional reprogramming is a distinct cancer hallmark, and specifying this transcriptional context can consistently and reliably reveal anti-tumor immune processes in cancer.

Limitations of the study

A number of single-cell RNA-seq profiles are used in the study to determine the levels of immune-like transcripts. Yet only a small proportion of immune transcripts were detected in individual cancer cells. This is

Table 3. Correlation between expression of CD83 and clinicopathological parameters

	CD83 negative		CD83 positive		
Parameters	NO.	%	NO.	%	p value
All patients	238	65.0	128	35.0	
Age, years					0.461
≤50	145	63.6	83	36.4	
>50	93	67.4	45	32.6	
Menopause					0.806
Premenopause	155	64.6	85	35.4	
Promenopause	83	65.9	43	34.1	
Tumor size, cm					0.053
≤2	78	58.6	55	41.4	
>2	160	68.7	73	31.3	
Node status					0.471
Negative	106	67.1	52	32.9	
Positive	132	63.5	76	36.4	
Histology type					0.888
Invasive ductal	224	65.1	120	34.9	
Others	14	63.6	8	36.4	
Tumor grade					0.725
1 or 2	67	59.3	46	40.7	
3	36	62.1	22	37.9	
Missing	135		60		
Stage					0.256
I or II	152	67.3	74	32.7	
III	86	61.4	54	38.6	
ER status					0.552
Negative	27	69.2	12	30.8	
Positive	210	64.4	116	35.6	
Missing	1				
PR status					0.621
Negative	36	67.9	17	32.1	
Positive	201	64.4	111	35.6	
Missing	1				
HER2 status					0.324
Negative	128	62.7	76	37.3	
Positive	109	67.7	52	32.3	
Missing	1				
Ki67					0.943
Negative	12	63.2	7	36.8	
Positive	134	62.3	81	37.7	
Missing	92		40		
Distant metastasis					0.181
Negative	187	63.4	108	36.6	
Positive	51	71.8	20	28.2	

caused by the limitation of current single-cell RNA-seq profiles, which cover only a proportion of genes in single cells. Indeed, the ssGSEA-based approach partially overcomes this limitation by evaluating gene sets instead of individual genes. Future efforts that improve the coverage of single-cell transcriptomes would be valuable to study the differentiation of plasticity in cancer. The immune mimicry of cancer cells is confirmed in single cancer cells and tumorigenesis models by data mining and *in vitro* models. Single-cell studies in more cancer models, especially *in vivo* tumorigenesis models and clinical samples, could strengthen this concept. The prognostic analyses with optimized immune response signature (oIRS) provide potential clinical biomarkers and therapeutic targets for cancer immunotherapy. This study addressed the problem of immune infiltration by integrating single-cell transcriptome, tumor mass transcriptome, and clinical parameters to determine the status of immune mimicry. Deciphering the immune-like transcripts provide an updated view on the tumor-immune interactions, which could be tested by future mechanistic and clinical studies.

STAR★METHODS

Detailed methods are provided in the online version of this paper and include the following:

- KEY RESOURCES TABLE
- RESOURCE AVAILABILITY
  - Lead contact
  - Materials availability
  - Data and code availability
- EXPERIMENTAL MODEL AND SUBJECT DETAILS
- METHOD DETAILS
  - Single-sample gene set enrichment analysis
  - Hierarchical clustering
  - Single cell analysis in Seurat
  - Cell culture
  - Flow cytometry
  - Western blot
  - Kaplan-Meier survival analysis
  - Expression profile analysis in GTEX, CCLE and GEO
  - Gene set enrichment analysis (GSEA)
  - Validation in TCPA dataset
  - Gene ontology annotation
  - Immunohistochemistry and scoring
- QUANTIFICATION AND STATISTICAL ANALYSIS

SUPPLEMENTAL INFORMATION

Supplemental information can be found online at https://doi.org/10.1016/j.isci.2021.103133.

ACKNOWLEDGMENTS

We would like to thank Quentin Liu's lab members for their critical comments and technical support. We also thank our colleagues for their collection/processing of patients' samples, as wells as all the patients for donating their samples. This research work was supported by the National Key R&D Program of China (2019YFA0110300), National Natural Science Foundation of China (No. 81970177, No. 82003096, No. 82002943 and No. 81972594), Natural Science Foundation of Guangdong (2017A030313608), the Science and Technology Planning Project of Guangzhou (201804020044).

AUTHOR CONTRIBUTIONS

R.G., and B.H. designed the research; R.G. and QT.H. performed the experiments; R.G., B.H. and ZF.W. executed bioinformatic analyses; R.G., B.H., M.Y. and E.WF.L. write the manuscript; Q.L., B.W. and SX.L. led the project and oversaw preparation of the manuscript.

DECLARATION OF INTERESTS

The authors declare no competing interests.

INCLUSION AND DIVERSITY

We worked to ensure diversity in experimental samples through the selection of the cell lines. We worked to ensure diversity in experimental samples through the selection of the genomic datasets. While citing references scientifically relevant for this work, we also actively worked to promote gender balance in our reference list.

Received: May 31, 2021
Revised: September 6, 2021
Accepted: September 10, 2021
Published: October 22, 2021

REFERENCES

Barbie, D.A., Tamayo, P., Boehm, J.S., Kim, S.Y., Moody, S.E., Dunn, I.F., Schinzel, A.C., Sandy, P., Meylan, E., Scholl, C., et al. (2009). Systematic RNA interference reveals that oncogenic KRAS-driven cancers require TBK1. Nature *462*, 108–112.

Barretina, J., Caponigro, G., Stransky, N., Venkatesan, K., Margolin, A.A., Kim, S., Wilson, C.J., Lehar, J., Kryukov, G.V., Sonkin, D., et al. (2012). The Cancer Cell Line Encyclopedia enables predictive modelling of anticancer drug sensitivity. Nature *483*, 603–607.

Bruni, D., Angell, H.K., and Galon, J. (2020). The immune contexture and Immunoscore in cancer prognosis and therapeutic efficacy. Nat. Rev. Cancer *20*, 662–680.

Chung, W., Eum, H.H., Lee, H.O., Lee, K.M., Lee, H.B., Kim, K.T., Ryu, H.S., Kim, S., Lee, J.E., Park, Y.H., et al. (2017). Single-cell RNA-seq enables comprehensive tumour and immune cell profiling in primary breast cancer. Nat. Commun. *8*, 15081.

Darmanis, S., Sloan, S.A., Croote, D., Mignardi, M., Chernikova, S., Samghababi, P., Zhang, Y., Neff, N., Kowarsky, M., Caneda, C., et al. (2017). Single-cell RNA-seq analysis of infiltrating neoplastic cells at the migrating front of human glioblastoma. Cell Rep. *21*, 1399–1410.

Elyada, E., Bolisetty, M., Laise, P., Flynn, W.F., Courtois, E.T., Burkhart, R.A., Teinor, J.A., Belleau, P., Biffi, G., Lucito, M.S., et al. (2019). Cross-species single-cell analysis of pancreatic ductal adenocarcinoma reveals antigen-presenting cancer-associated fibroblasts. Cancer Discov. *9*, 1102–1123.

Filbin, M.G., Tirosh, I., Hovestadt, V., Shaw, M.L., Escalante, L.E., Mathewson, N.D., Neftel, C., Frank, N., Pelton, K., Hebert, C.M., et al. (2018). Developmental and oncogenic programs in H3K27M gliomas dissected by single-cell RNA-seq. Science *360*, 331–335.

Francesconi, M., Di Stefano, B., Berenguer, C., de Andres-Aguayo, L., Plana-Carmona, M., Mendez-Lago, M., Guillaumet-Adkins, A., Rodriguez-Esteban, G., Gut, M., Gut, I.G., et al. (2019). Single cell RNA-seq identifies the origins of heterogeneity in efficient cell transdifferentiation and reprogramming. Elife *8*, e41627.

Gangoso, E., Southgate, B., Bradley, L., Rus, S., Galvez-Cancino, F., McGivern, N., Guc, E., Kapourani, C.A., Byron, A., Ferguson, K.M., et al. (2021). Glioblastomas acquire myeloid-affiliated transcriptional programs via epigenetic immunoediting to elicit immune evasion. Cell *184*, 2454–2470.e2426.

Gentles, A.J., Newman, A.M., Liu, C.L., Bratman, S.V., Feng, W., Kim, D., Nair, V.S., Xu, Y., Khuong, A., Hoang, C.D., et al. (2015). The prognostic landscape of genes and infiltrating immune cells across human cancers. Nat. Med. *21*, 938–945.

Gokce, O., Stanley, G.M., Treutlein, B., Neff, N.F., Camp, J.G., Malenka, R.C., Rothwell, P.E., Fuccillo, M.V., Sudhof, T.C., and Quake, S.R. (2016). Cellular taxonomy of the mouse striatum as revealed by single-cell RNA-seq. Cell Rep. *16*, 1126–1137.

Gorenshteyn, D., Zaslavsky, E., Fribourg, M., Park, C.Y., Wong, A.K., Tadych, A., Hartmann, B.M., Albrecht, R.A., Garcia-Sastre, A., Kleinstein, S.H., et al. (2015). Interactive big data resource to elucidate human immune pathways and diseases. Immunity *43*, 605–614.

Guillaumet-Adkins, A., Rodriguez-Esteban, G., Mereu, E., Mendez-Lago, M., Jaitin, D.A., Villanueva, A., Vidal, A., Martinez-Marti, A., Felip, E., Vivancos, A., et al. (2017). Single-cell transcriptome conservation in cryopreserved cells and tissues. Genome Biol. *18*, 45.

Gyorffy, B., Lanczky, A., Eklund, A.C., Denkert, C., Budczies, J., Li, Q., and Szallasi, Z. (2010). An online survival analysis tool to rapidly assess the effect of 22,277 genes on breast cancer prognosis using microarray data of 1,809 patients. Breast Cancer Res. Treat. *123*, 725–731.

Gyorffy, B., Lanczky, A., and Szallasi, Z. (2012). Implementing an online tool for genome-wide validation of survival-associated biomarkers in ovarian-cancer using microarray data from 1287 patients. Endocr. Relat. Cancer *19*, 197–208.

Gyorffy, B., Surowiak, P., Budczies, J., and Lanczky, A. (2013). Online survival analysis software to assess the prognostic value of biomarkers using transcriptomic data in non-small-cell lung cancer. PLoS ONE *8*, e82241.

Havel, J.J., Chowell, D., and Chan, T.A. (2019). The evolving landscape of biomarkers for checkpoint inhibitor immunotherapy. Nat. Rev. Cancer *19*, 133–150.

He, B., Gao, R., Lv, D., Wen, Y., Song, L., Wang, X., Lin, S., Huang, Q., Deng, Z., Wang, Z., et al. (2019). The prognostic landscape of interactive biological processes presents treatment responses in cancer. EBioMedicine *41*, 120–133.

Hodi, F.S., O'Day, S.J., McDermott, D.F., Weber, R.W., Sosman, J.A., Haanen, J.B., Gonzalez, R., Robert, C., Schadendorf, D., Hassel, J.C., et al. (2010). Improved survival with ipilimumab in patients with metastatic melanoma. N. Engl. J. Med. *363*, 711–723.

Hosein, A.N., Huang, H., Wang, Z., Parmar, K., Du, W., Huang, J., Maitra, A., Olson, E., Verma, U., and Brekken, R.A. (2019). Cellular heterogeneity during mouse pancreatic ductal adenocarcinoma progression at single-cell resolution. JCI Insight *5*, e129212.

Huang, D.W., Sherman, B.T., Tan, Q., Kir, J., Liu, D., Bryant, D., Guo, Y., Stephens, R., Baseler, M.W., Lane, H.C., et al. (2007). DAVID Bioinformatics Resources: expanded annotation database and novel algorithms to better extract biology from large gene lists. Nucl. Acids Res. *35*, W169–W175.

Iwamoto, M., Shinohara, H., Miyamoto, A., Okuzawa, M., Mabuchi, H., Nohara, T., Gon, G., Toyoda, M., and Tanigawa, N. (2003). Prognostic value of tumor-infiltrating dendritic cells expressing CD83 in human breast carcinomas. Int. J. Cancer *104*, 92–97.

Jordan, N.V., Bardia, A., Wittner, B.S., Benes, C., Ligorio, M., Zheng, Y., Yu, M., Sundaresan, T.K., Licausi, J.A., Desai, R., et al. (2016). HER2 expression identifies dynamic functional states within circulating breast cancer cells. Nature *537*, 102–106.

Karaayvaz, M., Cristea, S., Gillespie, S.M., Patel, A.P., Mylvaganam, R., Luo, C.C., Specht, M.C., Bernstein, B.E., Michor, F., and Ellisen, L.W. (2018). Unravelling subclonal heterogeneity and aggressive disease states in TNBC through single-cell RNA-seq. Nat. Commun. *9*, 3588.

Kim, K.T., Lee, H.W., Lee, H.O., Kim, S.C., Seo, Y.J., Chung, W., Eum, H.H., Nam, D.H., Kim, J., Joo, K.M., et al. (2015). Single-cell mRNA sequencing identifies subclonal heterogeneity in anti-cancer drug responses of lung adenocarcinoma cells. Genome Biol. *16*, 127.

Kim, K.T., Lee, H.W., Lee, H.O., Song, H.J., Jeong da, E., Shin, S., Kim, H., Shin, Y., Nam, D.H., Jeong, B.C., et al. (2016). Application of single-cell RNA sequencing in optimizing a combinatorial therapeutic strategy in metastatic renal cell carcinoma. Genome Biol. *17*, 80.

Li, H., Courtois, E.T., Sengupta, D., Tan, Y., Chen, K.H., Goh, J.J.L., Kong, S.L., Chua, C., Hon, L.K., Tan, W.S., et al. (2017). Reference component

analysis of single-cell transcriptomes elucidates cellular heterogeneity in human colorectal tumors. Nat. Genet. *49*, 708–718.

Li, J., Lu, Y., Akbani, R., Ju, Z., Roebuck, P.L., Liu, W., Yang, J.Y., Broom, B.M., Verhaak, R.G., Kane, D.W., et al. (2013). TCPA: a resource for cancer functional proteomics data. Nat. Methods *10*, 1046–1047.

Li, Z., Ju, X., Silveira, P.A., Abadir, E., Hsu, W.H., Hart, D.N.J., and Clark, G.J. (2019). CD83: activation marker for antigen presenting cells and its therapeutic potential. Front Immunol. *10*, 1312.

Maier, B., Leader, A.M., Chen, S.T., Tung, N., Chang, C., LeBerichel, J., Chudnovskiy, A., Maskey, S., Walker, L., Finnigan, J.P., et al. (2020). A conserved dendritic-cell regulatory program limits antitumour immunity. Nature *580*, 257–262.

Maniotis, A.J., Folberg, R., Hess, A., Seftor, E.A., Gardner, L.M., Pe'er, J., Trent, J.M., Meltzer, P.S., and Hendrix, M.J. (1999). Vascular channel formation by human melanoma cells in vivo and in vitro: vasculogenic mimicry. Am. J. Pathol. *155*, 739–752.

McMullen, T.P., Lai, R., Dabbagh, L., Wallace, T.M., and de Gara, C.J. (2010). Survival in rectal cancer is predicted by T cell infiltration of tumour-associated lymphoid nodules. Clin. Exp. Immunol. *161*, 81–88.

Miao, D., Margolis, C.A., Gao, W., Voss, M.H., Li, W., Martini, D.J., Norton, C., Bosse, D., Wankowicz, S.M., Cullen, D., et al. (2018). Genomic correlates of response to immune checkpoint therapies in clear cell renal cell carcinoma. Science *359*, 801–806.

Mlecnik, B., Bindea, G., Angell, H.K., Maby, P., Angelova, M., Tougeron, D., Church, S.E., Lafontaine, L., Fischer, M., Fredriksen, T., et al. (2016). Integrative analyses of colorectal cancer show immunoscore is a stronger predictor of patient survival than microsatellite instability. Immunity *44*, 698–711.

Muraro, M.J., Dharmadhikari, G., Grun, D., Groen, N., Dielen, T., Jansen, E., van Gurp, L., Engelse, M.A., Carlotti, F., de Koning, E.J., et al. (2016). A single-cell transcriptome Atlas of the human pancreas. Cell Syst. *3*, 385–394.e383.

Neftel, C., Laffy, J., Filbin, M.G., Hara, T., Shore, M.E., Rahme, G.J., Richman, A.R., Silverbush, D., Shaw, M.L., Hebert, C.M., et al. (2019). An integrative model of cellular states, plasticity, and genetics for glioblastoma. Cell *178*, 835–849.e821.

Newman, A.M., Liu, C.L., Green, M.R., Gentles, A.J., Feng, W., Xu, Y., Hoang, C.D., Diehn, M., and Alizadeh, A.A. (2015). Robust enumeration of cell subsets from tissue expression profiles. Nat. Methods *12*, 453–457.

Nguyen, Q.H., Pervolarakis, N., Blake, K., Ma, D., Davis, R.T., James, N., Phung, A.T., Willey, E., Kumar, R., Jabart, E., et al. (2018). Profiling human breast epithelial cells using single cell RNA sequencing identifies cell diversity. Nat. Commun. *9*, 2028.

Nishida, J., Momoi, Y., Miyakuni, K., Tamura, Y., Takahashi, K., Koinuma, D., Miyazono, K., and Ehata, S. (2020). Epigenetic remodelling shapes inflammatory renal cancer and neutrophil-dependent metastasis. Nat. Cell Biol. *22*, 465–475.

Ouadah, Y., Rojas, E.R., Riordan, D.P., Capostagno, S., Kuo, C.S., and Krasnow, M.A. (2019). Rare pulmonary neuroendocrine cells are stem cells regulated by Rb, p53, and notch. Cell *179*, 403–416.e423.

Postow, M.A., Chesney, J., Pavlick, A.C., Robert, C., Grossmann, K., McDermott, D., Linette, G.P., Meyer, N., Giguere, J.K., Agarwala, S.S., et al. (2015). Nivolumab and ipilimumab versus ipilimumab in untreated melanoma. N. Engl. J. Med. *372*, 2006–2017.

Salmon, H., Remark, R., Gnjatic, S., and Merad, M. (2019). Host tissue determinants of tumour immunity. Nat. Rev. Cancer *19*, 215–227.

Segovia, C., San Jose-Eneriz, E., Munera-Maravilla, E., Martinez-Fernandez, M., Garate, L., Miranda, E., Vilas-Zornoza, A., Lodewijk, I., Rubio, C., Segrelles, C., et al. (2019). Inhibition of a G9a/DNMT network triggers immune-mediated bladder cancer regression. Nat. Med. *25*, 1073–1081.

Shimasaki, N., Jain, A., and Campana, D. (2020). NK cells for cancer immunotherapy. Nat. Rev. Drug Discov. *19*, 200–218.

Subramanian, A., Tamayo, P., Mootha, V.K., Mukherjee, S., Ebert, B.L., Gillette, M.A., Paulovich, A., Pomeroy, S.L., Golub, T.R., Lander, E.S., et al. (2005). Gene set enrichment analysis: a knowledge-based approach for interpreting genome-wide expression profiles. Proc. Natl. Acad. Sci. U S A *102*, 15545–15550.

Szczerba, B.M., Castro-Giner, F., Vetter, M., Krol, I., Gkountela, S., Landin, J., Scheidmann, M.C., Donato, C., Scherrer, R., Singer, J., et al. (2019). Neutrophils escort circulating tumour cells to enable cell cycle progression. Nature *566*, 553–557.

Tirosh, I., Venteicher, A.S., Hebert, C., Escalante, L.E., Patel, A.P., Yizhak, K., Fisher, J.M., Rodman, C., Mount, C., Filbin, M.G., et al. (2016). Single-cell RNA-seq supports a developmental hierarchy in human oligodendroglioma. Nature *539*, 309–313.

Venteicher, A.S., Tirosh, I., Hebert, C., Yizhak, K., Neftel, C., Filbin, M.G., Hovestadt, V., Escalante, L.E., Shaw, M.L., Rodman, C., et al. (2017). Decoupling genetics, lineages, and microenvironment in IDH-mutant gliomas by single-cell RNA-seq. Science *355*, eaai8478.

Vuong, N.H., Cook, D.P., Forrest, L.A., Carter, L.E., Robineau-Charette, P., Kofsky, J.M., Hodgkinson, K.M., and Vanderhyden, B.C. (2018). Single-cell RNA-sequencing reveals transcriptional dynamics of estrogen-induced dysplasia in the ovarian surface epithelium. Plos Genet. *14*, e1007788.

Wang, H., Xiang, D., Liu, B., He, A., Randle, H.J., Zhang, K.X., Dongre, A., Sachs, N., Clark, A.P., Tao, L., et al. (2019). Inadequate DNA damage repair promotes mammary transdifferentiation, leading to BRCA1 breast cancer. Cell *178*, 135–151.e119.

Wculek, S.K., Cueto, F.J., Mujal, A.M., Melero, I., Krummel, M.F., and Sancho, D. (2020). Dendritic cells in cancer immunology and immunotherapy. Nat. Rev. Immunol. *20*, 7–24.

Weinstein, J.N., Collisson, E.A., Mills, G.B., Shaw, K.R., Ozenberger, B.A., Ellrott, K., Shmulevich, I., Sander, C., and Stuart, J.M. (2013). The cancer genome Atlas pan-cancer analysis project. Nat. Genet. *45*, 1113–1120.

Winterhoff, B.J., Maile, M., Mitra, A.K., Sebe, A., Bazzaro, M., Geller, M.A., Abrahante, J.E., Klein, M., Hellweg, R., Mullany, S.A., et al. (2017). Single cell sequencing reveals heterogeneity within ovarian cancer epithelium and cancer associated stromal cells. Gynecol. Oncol. *144*, 598–606.

Wu, H., Kirita, Y., Donnelly, E.L., and Humphreys, B.D. (2019). Advantages of single-nucleus over single-cell RNA sequencing of adult kidney: rare cell types and novel cell states revealed in fibrosis. J. Am. Soc. Nephrol. *30*, 23–32.

Yu, H., Lee, H., Herrmann, A., Buettner, R., and Jove, R. (2014). Revisiting STAT3 signalling in cancer: new and unexpected biological functions. Nat. Rev. Cancer *14*, 736–746.

Zeng, Q., Michael, I.P., Zhang, P., Saghafinia, S., Knott, G., Jiao, W., McCabe, B.D., Galvan, J.A., Robinson, H.P.C., Zlobec, I., et al. (2019). Synaptic proximity enables NMDAR signalling to promote brain metastasis. Nature *573*, 526–531.

STAR★METHODS

KEY RESOURCES TABLE

REAGENT or RESOURCE	SOURCE	IDENTIFIER
Antibodies		
anti-human CD68-FITC	BioLegend	Cat# 333805; RRID:AB_1089055
anti-human CD45-APC/Fire™ 750	BioLegend	Cat# 982314; RRID:AB_2832915
anti-human CD4-Brilliant Violet 605	BioLegend	Cat# 317437; RRID:AB_11204077
anti-human CD209-PE	BioLegend	Cat# 330105; RRID:AB_1134060
anti-human CD11B-Alexa Fluor®700	BioLegend	Cat# 301355; RRID:AB_2750074
anti-human/mouse FOXP3-Alexa Fluor® 647	BioLegend	Cat# 320013; RRID:AB_439749
Rabbit anti-human/mouse MYC	Proteintech	Cat# 10828-1-AP; RRID:AB_2148585
Mouse anti-Flag tag	Sigma-Aldrich	Cat# F1804; RRID:AB_262044
mouse anti GAPDH	Santa Cruz	Cat# sc-32233; RRID:AB_627679
Bacterial and virus strains		
pLVX-Tet3G	Addgene	#6111
pLVX-TRE3G	Addgene	#6113
psPAX2	Addgene	#12260
pMD2.G	Addgene	#12259
Biological samples		
Human breast cancer tissue	Sun Yat-Sen University Cancer Center	https://www.sysucc.org.cn/
Chemicals, peptides, and recombinant proteins		
Doxycycline	Sigma-Aldrich	D3072
Deposited data		
scRNA-seq of colorectal cells	Li et al., 2017	GSE81861
scRNA-seq of glioblastoma	Neftel et al., 2019	GSE131928
scRNA-seq of lung epithelial	Ouadah et al., 2019	GSE136580
scRNA-seq of lung adenocarcinoma	Kim et al., 2015	GSE69405
scRNA-seq of normal kidney tissue	Wu et al., 2019	GSE119531
scRNA-seq of kidney clear cell carcinoma	Kim et al., 2016	GSE73121
scRNA-seq of normal pancreatic cells	Muraro et al., 2016	GSE85241
scRNA-seq of pancreatic cancer	Elyada et al., 2019	GSE129455
scRNA-seq of normal brain cells	Gokce et al., 2016	GSE82187
scRNA-seq of glioma	Venteicher et al., 2017	GSE89567
scRNA-seq of oligodendroglioma	Tirosh et al., 2016	GSE70630
scRNA-seq of mouse breast tumor progression	Wang et al., 2019	GSE130453
scRNA-seq of trans-differentiating B cells	Francesconi et al., 2019	GSE112004
scRNA-seq of normal breast epithelial	Nguyen et al., 2018	GSE113099
scRNA-seq of breast cancer	Chung et al., 2017	GSE75688
scRNA-seq of breast cancer	Jordan et al., 2016	GSE75367
scRNA-seq of triple-negative breast cancer	Karaayvaz et al., 2018	GSE118389
scRNA-seq of normal ovarian tissue	Vuong et al., 2018	GSE121957
scRNA-seq of ovarian cancer	Winterhoff et al., 2017	GSE123476
scRNA-seq of ovarian cancer	Guillaumet-Adkins et al., 2017	GSE85534

(*Continued on next page*)

Continued

REAGENT or RESOURCE	SOURCE	IDENTIFIER
scRNA-seq of glioblastoma	Filbin et al., 2018	GSE102130
scRNA-seq of glioblastoma	Darmanis et al., 2017	GSE84465
scRNA-seq of mouse pancreatic progression	Hosein et al., 2019	GSE125588
RNA-seq in tissues from patient with immunotherapy	Segovia et al., 2019	GSE111636
RNA-seq in tissues from patient with immunotherapy	Miao et al., 2018	Aa5951
Experimental models: cell lines		
Human: MCF-10A cell line	ATCC	CRL-10317
Recombinant DNA		
pLVX-HRASG12V-TRE3G	This manuscript	N/A
pLVX-MYC-TRE3G	This manuscript	N/A
pLVX-ERBB3-TRE3G	This manuscript	N/A
Software and algorithms		
R 4.1.0	R Development Core Team	Version 4.1.0
Seurat 3.0.0	https://github.com/satijalab/	
seurat/releases/tag/v3.0.0	Version 3.0.0	
ssGSEA	https://www.genepattern.org/	Version 1.0
Cluster 3.0	http://bonsai.ims.u-tokyo.ac.jp/mdehoon/software/cluster	Version 3.0
Treeview	https://treeview.software.informer.com/1.6/	Version 1.6
GSEA	https://www.gsea-msigdb.org/gsea/index.jsp	https://www.gsea-msigdb.org/gsea/index.jsp
GraphPad PRISM	https://www.graphpad.com/	Version 9.0.0
SPSS	https://spss.en.softonic.com/	Version 16.0

RESOURCE AVAILABILITY

Lead contact

Further information and requests for resources and reagents should be directed to and will be fulfilled by the lead contact, Dr. Quentin Liu (liuq9@mail.sysu.edu.cn).

Materials availability

Materials used or generated in this study will be available upon reasonable request.

Data and code availability

This paper analyzes existing, publicly available data. These accession numbers for the datasets are listed in the key resources table. This paper does not report original code. Any additional information required to reanalyze the data reported in this paper is available from the lead contact upon request.

EXPERIMENTAL MODEL AND SUBJECT DETAILS

MCF-10A cells were obtained from ATCC. Dox inducible MCF-10A cell lines were constructed using lentivirus containing HRASG12V, ERBB2 or MYC-encoding vectors (parental backbone was pLVX-TRE3G (Addgene, #6113). Infected MCF-10A cells were selected by puromycin (1.2 μg/mL for 5 days). The study in human breast cancer tissues was approved by the ethical committee of Sun Yat-Sen University Cancer Center (#GZR2020-059). Paraffin-embedded samples of breast carcinoma tissues were obtained from 366 patients (January 2001 to October 2008) at Sun Yat-Sen University Cancer Center. All samples were collected with signed informed consent according to the internal review and ethics boards of Sun Yat-Sen University Cancer Center.

METHOD DETAILS

Single-sample gene set enrichment analysis

To perform single-sample gene set enrichment analysis (ssGSEA), gene expression data (single-cell gene expression matrix or bulk gene expression data) were submitted to the GenePattern platform. The ssGSEA Projection program (V9.0) was used to calculate individual enrichment scores for each pairing of a sample and a gene set. Gene sets of cellular markers, ISF, antigen presentation, T cell signaling and NK cell killing were loaded for enrichment analysis.

Hierarchical clustering

Gene expression, z-scores and normalized enrichment scores (NES) were subjected to Cluster 3.0 software. Both gene set and cancer type were clustered by average linkage. A clustered heat map was analyzed and visualized by TreeView.

Single cell analysis in Seurat

Cells were clustered and analyzed using customized codes based on the Seurat V4.0 package on R4.1.0. We followed the standard workflow in Seurat, as cells with less than 200 genes, 2,500 transcripts, or a mitochondrial level of 5% or greater were removed in the QC process. "LogNormalize" method was used to normalized the gene expression for each cell by the total expression, multiplying by a scale factor 10,000 and log-transforming the results. PCA was run using the previously determined most variably expressed genes for linear dimensional reduction. JackStraw resampling method was implemented by permutation on a subset of data (1% by default) and rerunning PCA for a total of 100 replications to select the statistically significant principle component (PC) for the K-nearest neighbors clustering. For graph-based clustering, the first 15 PC and a resolution of 3 were selected yielding distinct cell clusters. Treating the signature score of each cell type as a pseudogene, we evaluated the signature score for each cell in our dataset using the MetaFeature function. Signatures used to type cells included Klk1, Pnlip, Spink1 (acinar cells), Krt19, Krt7, Wfdc2 (ductal cells), Cd68, Cd14, Cd33, Itgam, Mrc1 (monocytes).

Cell culture

MCF-10A cells were maintained with DMEM/F12 medium with 5% horse serum, Insulin (10 μg/ml), EGF (20 ng/ml), Cholera Toxin (100 ng/ml) and Hydrocortisone (0.5 μg/ml). Genes for over-expression were constructed by inserting cDNA of candidate genes into pLVX-TRE3G (Addgene, #6113). Doxycycline (Dox) inducible constructs were used in combination with pLVX-Tet3G (Addgene, #6111). Dox inducible MCF-10A cell lines were constructed by puromycin selection after lentivirus infection. Dox (0.2 μg/ml) was used to induce oncogene expression in stable cell lines.

Flow cytometry

Cells were collected by trypsin, resuspended into single cell suspensions. For antibody staining, cells were washed with PBS once before staining with fluorescent antibodies (anti-human CD68-FITC, anti-human CD45-APC/Fire™ 750, anti-human CD4-Brilliant Violet 605, anti-human CD209-PE, anti-human CD11B-Alexa Fluor®700 and anti-human FOXP3-Alexa Fluor® 647) 30 min on ice, washed with ice cold PBS, resuspended in PBS and load for analysis.

Western blot

Cells or tissues were lysed using in RIPA (20 mM Tris pH 7.4; 150 mM NaCl, 1% Triton X-100, 0.5% sodium deoxycholate, 0.1% SDS, 5 mM EDTA, plus freshly added protease inhibitor cocktail). Protein quantification of lysates was performed using Bradford assay with Coomassie brilliant blue G-250. Lysates were prepared and electrophoresed using 10% SDS-polyacrylamide gels, and transferred to Immobilon-P PVDF membranes (Millipore). PVDF membranes were blocked with 5% BSA/TBST for 1 hr at room temperature prior to overnight incubation with indicated antibodies at 4°C. Western blots were probed with the following antibodies: total α-MYC (1:2000, Proteintech), α-Flag tag (1:5,000, Sigma-Aldrich). Antibodies to GAPDH (1:5,000, Santa Cruz) antibodies were used as controls. Proteins were visualized with ECL (Amersham) according to manufacturer's protocols.

Kaplan-Meier survival analysis

Gene symbol was inspected in the Kaplan Meier plotter online database (http://kmplot.com/analysis/index.php?p=background) (Gyorffy et al., 2012, 2013). User selected probe set was selected, and patients were split according to the optimized cut-offs. Relapse free survival of breast cancer, overall survival of lung, gastric and ovarian cancer was evaluated in all patients available in the database.

Expression profile analysis in GTEX, CCLE and GEO

Five hundred and forty-seven CIBERSORT signature genes were downloaded from the CIBERSORT database (http://cibersort.stanford.edu/) (Newman et al., 2015). Expression levels of the CIBERSORT genes in the GTEX project and single-cell transcriptomic data were downloaded from the Gene Expression Omnibus (GEO) database. Expression of CIBERSORT genes in CCLE was analyzed in the GENE-E tool of the CCLE database (Barretina et al., 2012) (http://www.broadinstitute.org/ccle/data/browseAnalyses). Genes were selected using the filter in GENE-E, followed by average linkage-based hierarchical clustering of the selected genes across cell lines and subjected to GENE-E analysis.

Gene set enrichment analysis (GSEA)

For GSEA in Aa5951 and GSE111636, patients were grouped into responder and non-responder groups according to the published information. Gene sets were analyzed by comparing the transcriptional profiles between subgroups of patients in the GSEA software (www.broadinstitute.org/gsea) (Subramanian et al., 2005). Significantly enriched gene sets were defined using a false discovery rate of q-value equals 0.25 and a nominal p value 0.05. All analyses were performed using GSEA v2.2.1 software with pre-ranked list and 1000 data permutations.

Validation in TCPA dataset

Markers for the enriched biological processes (e.g. immune cell differentiation and activation, etc.) were examined in the webpage survival analysis of the Cancer Proteome Atlas project (Li et al., 2013) (TCPA, http://app1.bioinformatics.mdanderson.org/tcpa/_design/basic/index.html).

Gene ontology annotation

Gene lists of interest were submitted to the DAVID Bioinformatics Resources 6.7 for annotation (https://david.ncifcrf.gov/summary.jsp) (Huang et al., 2007). Gene Ontology terms of biological process (GOTERM_BP_FAT), molecular function (GOTERM_MF_FAT) and cellular component (GOTERM_CC_FAT) were studied in the submitted lists.

Immunohistochemistry and scoring

Paraffin-embedded samples were sectioned at a thickness of 4 μm. Antigen retrieval was performed by a microwave oven for 15 min in EDTA (PH 8.0), followed by treatment with 3% H_2O_2 for 15 min. Specimens were incubated with antibodies specific for CD83 (Cat.NO. sc-19677, Santa Cruz; 1:50) overnight at 4°C. Envision Detection system (DAKO) was used to detect antigen expression according to the manufacturer's instructions. Isotype-matched antibodies were applied as negative controls. CD83 + dendritic cells were calculated per field of view, with at least 5 view-fields per section evaluated at 400× magnification. Infiltration scores were evaluated by calculating average CD83 + cells per field. Scoring was performed by two independent observers who were blind to clinical outcome.

QUANTIFICATION AND STATISTICAL ANALYSIS

Survival analysis was performed using SPSS version 16.0 (SPSS Inc.) and GraphPad Prism version 9. Kaplan–Meier statistics and log rank (one-tail) tests were performed to estimate the significance of differences in overall survival and disease-free survival of patients between groups. Other p values were determined using two-tailed Student's *t* test or two-sided Mann Whitney Wilcoxon test. Significant results were defined when $p < 0.05$.